RADIATIVE LIFETIME AND INTERNAL QUANTUM EFFICIENCY OF SMALL SCALE SILICON NANOSTRUCTURES

SUBMITTED IN PARTIAL FULFILLMENT OF THE
REQUIREMENTS FOR THE DEGREE OF
MASTER OF SCIENCE IN PHYSICS
AT
ADDIS ABABA UNIVERSITY
ADDIS ABABA, ETHIOPIA
JUNE 2009

By

Sioma Debela

Table of Contents

List of Figures

Acknowledgements

First of all I need to thank my God for all. Next, I would like to thank Dr. Sib Krishna Ghoshal, my instructor and advisor, for his advice during this research. His effort in providing the necessary materials for the accomplishment of this thesis gives me a great pleasure.

I indebted to my brother John Debela and my cousin Sara Tariku for their constant financial support and courage during my M.SC. studies. Thank you John, thank you Sara. I would also like to acknowledge my brother Michael Debela and my mother Ayelech Damtew for their constant courage.

Abstract

Nanosilicon (nanocrystal and porous) research is gaining tremendous attention in recent years due to the light emitting properties of the material. Improving efficiencies in radiative recombination and light extraction of this material enhances potential applications as microelectronic and optoelectronic devices with new operational capabilities. In this work we investigate the influence of quantum confinement and excitation laser pump flux on the optical parameters of silicon nanocrystal. Our work presents a new approach for the photoluminescence mechanism of silicon nanocrystal by using phenomenological formulations that explain the size and laser pump flux dependence of photoluminescence intensity, radiative lifetime and internal quantum efficiency. To investigate the mechanism of the photoluminescence we perform computer simulation using fortran programming. These results show that, miniaturizing the size and increasing laser pump flux strongly alters photoluminescence intensity, radiative lifetime and internal quantum efficiency of silicon nanocrystal. Our results have in well agreement with many other theoretical and experimental findings. Our model confirms photoluminescence emission intensity and internal quantum efficiency enhance due to quantum confinement and we can tune the emission spectral range across the visible by using proper sized silicon nanocrystal.

Chapter 1

Introduction

Silicon is the most widespread semiconductor in modern microelectronics technologies. Its natural abundance, low cost and high purity, as well as the high electronic quality of the si/sio_2 interface, have led to its over whelming dominance in microelectronic devices [1]. It is observed in figure 1.1 that the rise in the number of publications witnessing the rising interest in this material.

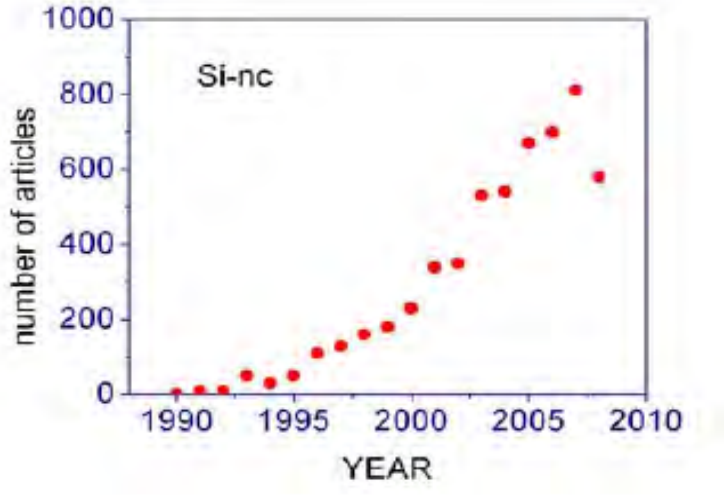

Figure 1.1: The rising interest in silicon can be observed if one gets look for nc-si in Google scholar (adapted from [12]).

The grand success of silicon technology is not only the dramatic improvement that have been achieved in performance, but also the exponentially decreasing per-component manufacturing costs that have kept that performance affordable [2]. It has become cheaper

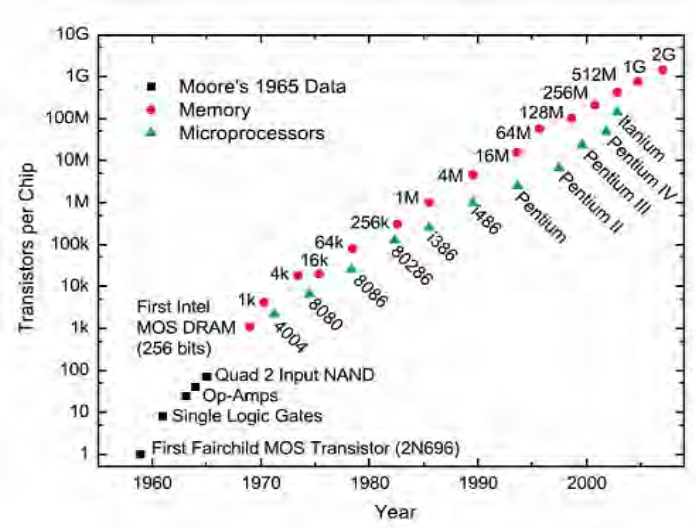

Figure 1.2: Transistor counts for integrated circuits showing the historical accuracy of Gordon Moores prediction of exponentially increasing integrated circuit complexity. (adapted from [2]).

over time to pack more and more transistors into integrated circuits because each individual transistor is continually being made smaller, the semiconductor industry progress predicted by Moore's low (the complexity for minimum component cost has increased at a rate of roughly a factor of two per years..., this rate can be expected to continue...) has been maintained through the present day (figure 1.2).

Today the total length of interconnecting conductors with in the chip reach as 20 Km (figure 1.3) [3]. As the number of transistors in an integrated circuit increases, more and more interconnecting wires must be included in the chip to link those transistors together, therefore communication inside a chip will become a serious obstacle to the continuation of the growth of the integrated circuits.

Nevertheless, the use of si in optoelectronic remains highly limited. This state of affairs has remained, in fact, almost unchanged because of fundamental property of the si band structure-the indirect band gap. In indirect band gap semiconductors like silicon there is a mismatch in momentum space between the electrons and holes states. To conserve momentum, excitation and relaxation between the conduction band and valence band

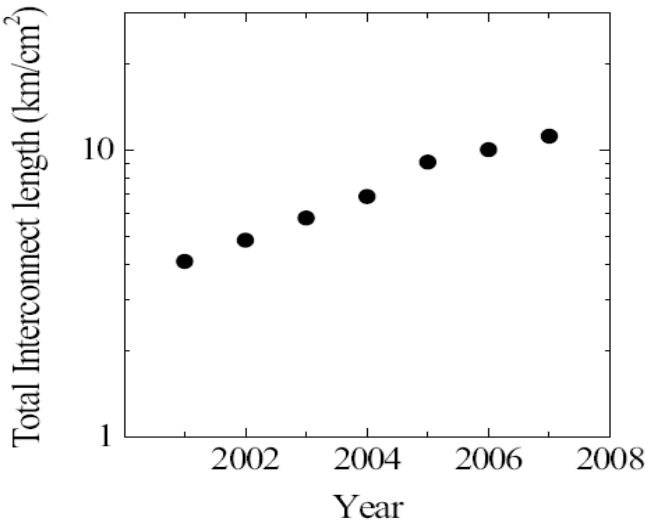

Figure 1.3: Total interconnect length inside a chip, for active wiring only, per square centimeter of active area (adapted from[16]).

extrema require the assistance of a crystal lattice vibration. Radiative recombination of excited charge carriers is therefore three-body process, and as a result, it is much less efficient than the analogous two-body recombination in a direct band gap semiconductor, where the conduction and valence band extrema are matched in momentum space. The low probability of radiative recombination in indirect band gap materials favors non radiative decay process, and excited electrons generally loose energy as heat, but not by emitted photons. These materials exhibit only very faint luminescence, even at low temperature, and this weakness has traditionally prevented the desirable extension of silicon microelectronics to silicon optoelectronics.

Some of the problems associated with the si band structure might be overcome in nanoscale crystallites hosted in a wide gap dielectric matrix like sio_2, in order to create a strong confining potential for carriers inside the nanocrystal. Electronic states become localized with in the nanocrystal and the momentum distribution spreads due to the Heisenberg uncertainty relation. Nanoscale silicon crystal exhibits efficient photoluminescence at visible energy above the silicon band gap of 1.12 eV. Radiative recombination is a much more efficient process in silicon nanocrystals than bulk silicon, however the power

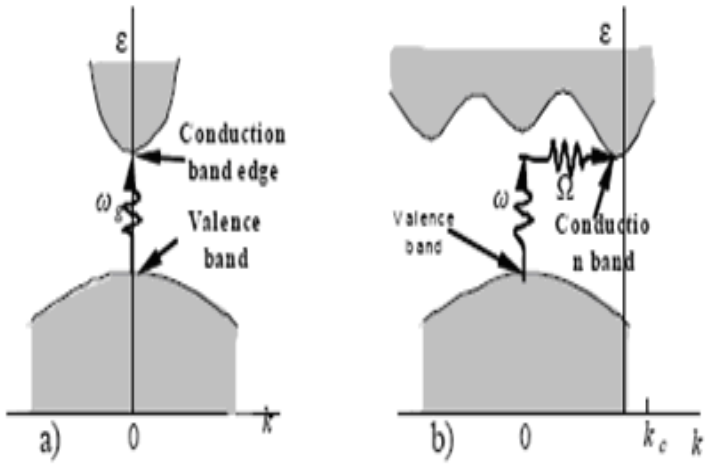

Figure 1.4: The transition of charge carries from valence band to conduction band is two and three-body process in direct (a) and indirect (b) band gap semiconductors respectively.

and emission quantum efficiency in si nanocrystals (nc-si) remains law compared to direct gap materials.

In order to compete with such direct band gap quantum dots as CdSe and InAs, the emission intensity of nc-si must be enhanced by three order of magnitude [4]. Thus, improvement of light emission efficiency of si quantum dots remains a challenge for opto-electronic technologies.

1.1 Quantum confinements effect by the size of nanostructures

Nanometer-sized semiconductor nanoparticles have attracted much interest for the last two decades as they possess unique physical and optical properties that are closely related to their size [5]. These nanoparticles are expected to exhibit quantum confinement effect when their size become comparable to Bohr exciton radius, which results in an increase in the energy gap related to that of the bulk solid. Once crystal size is decreased below a critical size, the continuous bands of the bulk semiconductor turn in to discrete atomic-like

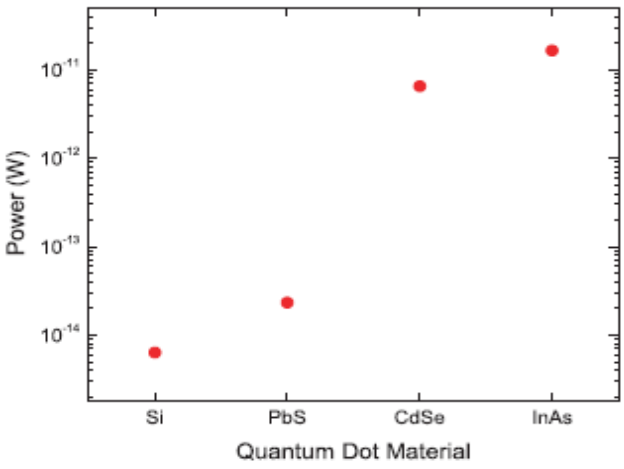

Figure 1.5: Comparison of emission power from four different direct gap semiconductor nanocrystals with nc-si adapted from [4]

energy levels and the band gap increases as size decreases due to quantum confinement, however the band gap increases appreciably only in the domain of extremely small sizes of the nanocrystals is reduced below the Bohr exciton radius, $a_0 = \frac{\epsilon\hbar^2}{4\pi^3\mu e^2}$ of the material, in silicon this length is 4.9 nm. The band gap increase is most easily observed in the UV-visible absorption spectra as the absorption edge shifts systematically to lower wave lengths [6]. An analytical model, introduced by Brus in 1986, in the assumption of an infinite potential out side the nanocrystal and zero potential inside, predicted that the quantum confinement effect in nanocrystals scales with confinement radius r. The expected energy-size relation ship or the blue shift of energy in the reduced mass picture is $\triangle E = (\frac{\hbar^2\pi^2}{2\mu})\frac{1}{r^2} - \frac{1.8e^2}{4\epsilon\varepsilon_0 r}$. The relative dielectric constant is given by ϵ and the reduced mass ($\mu^{-1} = m_e^{-1} + m_h^{-1}$). Where m_e and m_h are the electron and hole effective mass respectively, e is the electron charge and $\hbar$ is the reduced planck's constant.

The first term corresponds to the kinetic energy for the non interacting electron and hole in a spherical box of radius r. The second term arises due to the coulomb interaction between the electron and hole

However, the blue shift energy $\triangle E$, determined from experiments, does not obey the

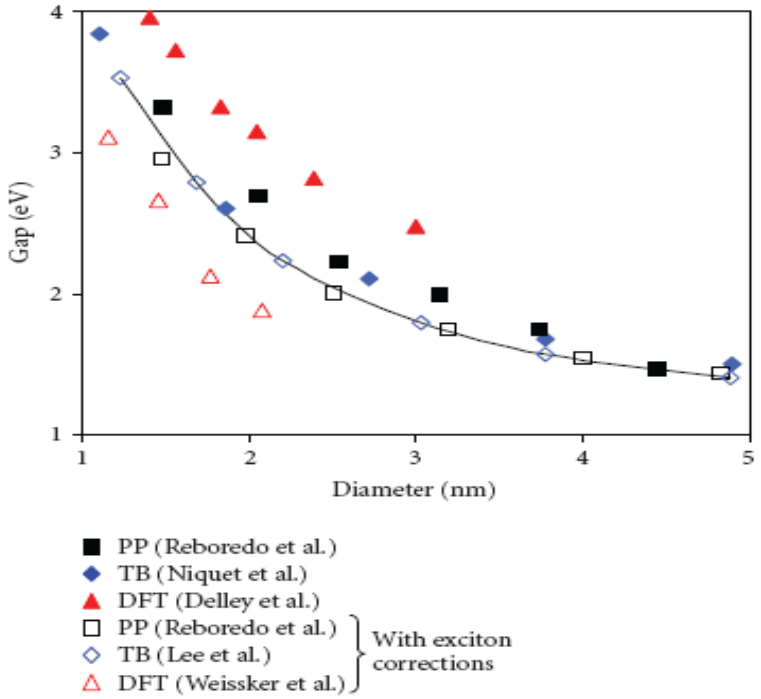

Figure 1.6: Optical gap calculated by pseudo potential (PP), tight binding (TB) and density functional theory (DFT) methods (adapted from [1])

law $\frac{c}{r^2}$ following from the simplest quantum mechanical model. This dependence is rather $\triangle E \sim r^{-x}$ with $1 < x < 1.5$ or an even weaker dependence on r in some cases [1, 7].

1.2 Density of States (DOS) of silicon nanostructures

In this section we are going to discuss how the density of states vary as we go from bulk to silicon nanocrystalline quantum structures i.e the electron density of states of a quantum dot (0D), quantum wire (1D), quantum well (2D) and bulk silicon (3D).

In order to characterize the physical properties like optical transitions, charge transport etc. The information about the density of states is very crucial. The density of states depends on the dimensionality of the system and the energy versus the corresponding wave vector dispersion relation for the system at hand.

For parabolic approximation of the energy versus the corresponding wave vector dispersion relation for the electron or hole we can take a simpler form. Therefore, for a

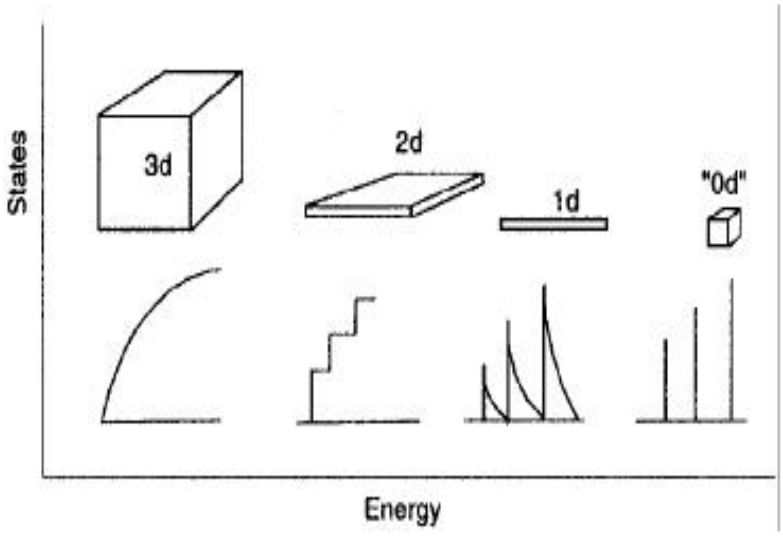

Figure 1.7: Density of states for various geometries of semiconductor materials:bulk (3-D), quantum well (2-D), quantum wire(a 1-D structure), and quantum dot (a 0-D entity). Adapted from [20]

three-dimensional bulk material, the DOS is defined as the number of available electronic states per unit volume per unit energy at energy E and is given by.

$$g(E) = \frac{\sqrt{2}m_e^{\frac{3}{2}}}{\pi^2\hbar^3}E^{\frac{1}{2}}$$

Passing from three-dimensional bulk to two-dimensional structures, (so called quantum well) the carrier movement is restricted to a plane. Such two-dimensional systems include thin films, layer structures and super lattices. Now the DOS is modified to the number of available electronic states per unit area per unit energy and is given by

$$g(E) = \frac{m_e}{\pi^2\hbar^2}$$

Further reduction in the dimensionality of the system ends up in a quantum wire. Examples of such one-dimensional structures include nanotubes, semiconductor nanowires, and nanorods. For a quantum wire the DOS is defined as the availability of electronic states per unit length per unit energy and is given by

$$g(E) = \frac{\sqrt{2} m_e^{\frac{-1}{2}}}{\pi \hbar} E^{\frac{-1}{2}}$$

Finally, for a zero dimensional system (QD), the confinement is along all three dimensions and the DOS becomes a delta function. Figure 1.4 schematically shows the modifications in the DOS as a function of dimension.

Transformation from a 3-D bulk system to a 2-D thin film changes the DOS from a continuous parabolic dependence to a step like dependence. This is due to the quantization of carrier motion in the thickness direction. Consequently the optical absorption edge is shifted to higher energy with respect to the bulk and above the absorption edge; the spectrum is stepped rather than smooth.

1.3 Photoluminescence

Electrons are excited across the band gap, from the valence band to the conduction band, by providing an appropriate energy greater than the band gap of the material. These excited electrons must decay back to the valence band by radiative or non -radiative thermal process. Non-radiative process is predominant routes to de-excitation when the electron-phonon coupling is strong. Phonon coupling provides quasi continuous states which the electrons can occupy successively to de-excite to the ground state. In the absence of strong phonon coupling, the electrons have to make a radiative transition that often correspond to energies close to the visible region of the electromagnetic spectrum. This phenomenon, known us photoluminescence. Photoluminescence can occur in nanocrystals in a variety of ways ;for example, the electron-hole recombination can take place by involving the electronic states at the band edge, surface, defect and other trap states, or states on doped impurity atoms, giving rise to photoluminescence at different energies for the same material [8].

Electrons can de-excite radiatively by a transition from the bottom of the conduction

band to the top of valence band. In the absence of any significant trap states, the energy absorbed by the system to create an electron -hole pair will necessarily be equal to the energy emitted, when the electron and the hole recombine without the loss of any energy prior to the emission. The presence of un quenched dangling orbitals at the surface or any defect states in the bulk, provide traps for the excited electrons and the holes prior to their recombination . These orbitals have their energies in the band gap regions. Therefore, an electron excited to the conduction band can transfer itself non-radiatively to one of these surface or defect states before making radiative transition to a lower energy states, likewise, a hole excited in the valence band can move in to the defect states depending up on the donor/acceptor character of the defect states. The net result of such non-radiative transfers of electrons and holes to lower energy states prior to radiative recombination is that the emission occurs at energies much lower than the band gap energy of the nanocrystals, in contrast to the band edge recombination considered earlier. This is often referred to as the red-shifted emission in nanocrystals.

1.4 Nanostructure fabrication methods

There are a variety of techniques that are capable of creating nanostructures with various degrees of quality, speed and cost. These approaches fall under two categories "bottom-up" and "top-down". Top-down approaches use patterning followed by etching or deposition, while bottom-up synthesis converts chemical reactants to nanomaterials. Although both approaches provide control over, size, shape, composition and surface chemistry, the bottom-up approach has more advantages. It facilitates the large scale, low-cost manufacturing of dispersible nanomaterials for low temperature processing, deposition on plastic substrates, mixing with molecular and polymeric materials in coating and composites, and even interfacing with living organisms for medical applications [9].

A diagram illustrating some of the types of materials and products that these two approaches are used for is shown in Figure 1.6

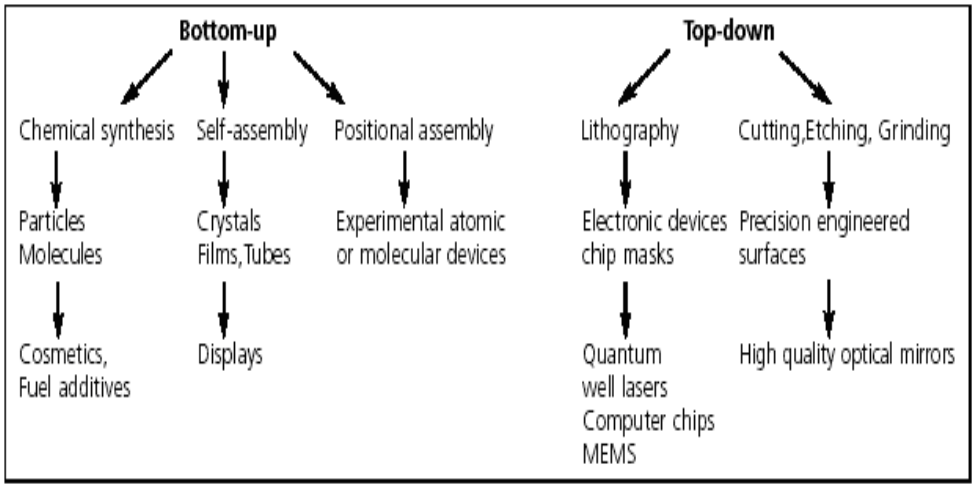

Figure 1.8: The use of bottom-up and top-down techniques in manufacturing.

The template method is one commonly used approach to obtain ordered array of one-dimensional nanostructures. As a well established nanotemplate, porous anodic alumina has been widely used to fabricate many kinds of nanowires and nanotubes, especially after the great improvement in pore regularity achieved using two-step anodization process [6]. Other methods for fabrication of ordered arrays include electron beam lithography, nanoimprint, and self assembly process. However, there are fabrication and application restrictions for these methods, such as limited pattern area and low through put, high equipment capital costs, and limited classes of materials that can be pattern large areas of surface. Additionally, template methods allow for deposition of a wide range of materials [6].

Moving away from the trial-and-error recipes the field of nanomaterials chemistry has evolved a fundamental understanding of synthesis with control shape and size [9].

1.5 Applications of silicon nanostructure

The possibility of tuning nanocrystals to desired absorption or emission wavelengths and many other good optical and electronic properties favors nanostructures for applications in LEDs, lasers, electronic devices and photovoltaics. In particular their good quantum

yield, narrow emission line-width and stability against bleaching have made them popular as near-infrared fluorescent tags for biological studies.

Silicon nanostructures with reduced dimensionality such as for example quantum wires, and quantum dots are attracting increasing attention both as object of basic research and as promising materials for the fabrication of devices with new operational capabilities that can not be attained using traditional semiconducting materials. These materials are very important and promising in the manufacture of light-emitting diodes, high mobility transistors, sensors, monochromatic light sources, wave guides, photonic studies, data storage devices and etc. The wide spread use of these materials and other related compound semiconductor materials light wave communication systems has resulted in intensive research in to the growth of these materials using a number of techniques.

In many application of nanostructured materials, such as microelectronics, optoelectronics, and sensing the ability to fabricate nanostructures with a huge degree of regularity and uniformity is important in achieving tight control of their property [6].

1.6 Objective

Our work is looking at methods to alter luminescence behavior of nanocrystalline silicon by improving internal quantum efficiency and radiative lifetime.

Specifically, we investigate the effect of size and excitation laser pump flux on radiative lifetime, internal quantum efficiency and PL intensity of nanocrystalline silicon based on quantum confinement and surface polarization models. Additionally for a given excitation frequency the diameter of nanocrystalline silicon associated with peak value of optical parameters is also investigated. Therefore we present a phenomenological description of optical parameters.

1.7 Thesis outline

In this thesis we study the optical transition between HOMO-LUMO states of silicon nanocrystal based on quantum confinement and surface polarization models. The thesis is organized in to five chapters.

Chapter 2 presents the optical properties of nanosilicon. Dielectric constant and refractive index reduction, oscillator strength, quantum efficiency and non-linear optical responses of nanosilicon are the main issues of this chapter.

Chapter 3 presents analytical calculations for optical parameters. It is shown that miniaturizing the size alters PL intensity, radiative lifetime and internal quantum efficiency of silicon nanocrystal. We further show the advantage of increasing laser pump flux on PL intensity, radiative lifetime and internal quantum efficiency. Thus we show analytically effect of laser pump flux on these optical parameters.

Chapter 4 Discusses the impact of miniaturizing the size and using high excitation laser pump flux based on results of our analytical calculations, we then compare our simulations with experimental results.

chapter 5 Contains the summary, conclusion and future directions for research in temperature dependent calculations.

Chapter 2

Optical properties of silicon nanostructure

In this chapter we are going to present how the optical properties vary as we go from bulk to nanosilicon.

2.1 Dielectric constant

Miniaturizing a semiconductor down to nanometer scale causes the dielectric constant ε_r of the semiconductor to decrease with the size [10, 11]. The reduced ε_r has enormous impact on the optical and electrical performance of the solid and the related devices. For instance the reduction in ε_r enhances the coulomb interaction between the charged particles such as electron, holes, and ionized shallow impurities in nanometric devices, leading to abnormal response of the devices [10, 11]. The increase in the energies for exciton activation in nanometric semiconductors due to ε_r reduction would significantly influence optical absorption and transparent property of this devices.

The smaller is the nc-si, the lower the refractive index. The actual value depends strongly on the dielectric in which nc-si are formed. In a simple scheme, the refractive index considered an average of the one of the matrix and the one of silicon weighted by the volumetric fraction of the law components. In reality the situation is more complex and the size of nc-si is relevant.

The static dielectric constant originates from the electric polarization, or electron transition from the lower valence band to the upper conduction band. This process is subject to the selection rule of energy and momentum conservation, which determines the optical response of semiconductors and reflects how strong the valence electron couple with the excited conduction electrons. Therefore the ε_r of a semiconductor is directly related to its E_g at room temperature.

There have been several models to describe the size dependence of the real part of the dielectric constant ε_r of the nanosolid with diameter d. The quantum confinement theories for nanodots are based on the generalized Penn model (GPM), expressed as

$$\varepsilon(r) = 1 + \frac{\varepsilon_{bulk} - 1}{1 + (\frac{\alpha}{r})^l} \tag{2.1.1}$$

Where r is the radius of the nanodots. On the other hand, the surface polarization effect theory considers a nanostructure to have two regions, surface and core with different dielectric values. The surface region of depth $d_{surface}$ (equivalently volume $V_{surface}$) has the dielectric value of $\varepsilon_{surface}$, whereas the rest of the region (core) that of ε_{bulk} . The dielectric value of an isolated nanoslab with two surface regions (one on each surface) as a whole then becomes

$$\varepsilon_r = \varepsilon_{bulk} - \frac{s}{r} \tag{2.1.2}$$

Where $2r$ is defined to be the total slab thickness and $s = (\varepsilon_{bulk} - \varepsilon_{surface})d_{surface}$. Noteworthy is the similarity between the surface polarization effect and the first order approximation of the GPM.

$$\varepsilon(r) = \varepsilon_{bulk} - (\varepsilon_{bulk} - 1)(\frac{\alpha}{r})^l \tag{2.1.3}$$

Which is formulated by expanding the GPM as a power series given $(\frac{\alpha}{r})^l < 1$ for all r of interest. From equation 2.1.3 the surface polarization effect expression can be obtained

by setting l=1 and replacing $\varepsilon_{bulk} - 1$ with $\varepsilon_{bulk} - \varepsilon_{surface}$. It is to be noted that the two computing theories both exhibit $(\frac{1}{r})^l$ dependence [10, 11].

The imaginary part of the complex dielectric constant ε_r describes the EM wave absorption and is responsible for the energy loss of incident irradiation by electron excitation. The imaginary part of complex dielectric constant can be obtained by Kramers-Kroning relation which correlates the real part to the imaginary part of dielectric constant.

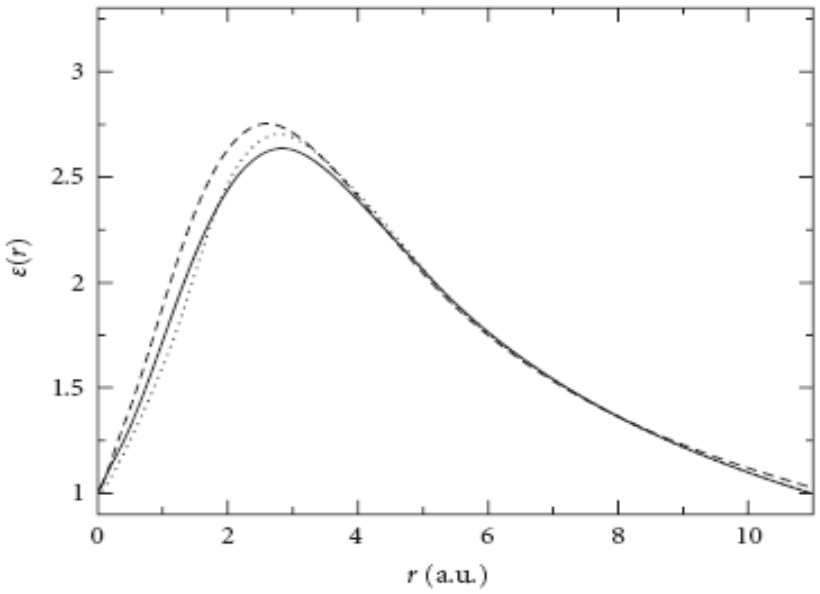

Figure 2.1: Dielectric function of silicon nc-si in silicon dioxide matrix $(\epsilon_d = 3)$ for (1) R = 1nm; (2) R = 1.75 nm; (3) R = 2.5nm (adapted from [1]).

2.2 Quantum efficiency

Light emission in bulk Si is phonon-mediated, with a very low probability because the spontaneous recombination lifetimes are in the millisecond range. The competitive non-radiative rates are much higher than the radiative ones, and most of the e-h pairs recombine non-radiatively. The quantum efficiency for Si luminescence is very low ($\sim 10^{-6}$). Bulk Si does not have lasing action because the fast non-radiative processes such as Auger or free-carrier absorption strongly prevent population inversion at the high pumping rates needed to achieve optical amplification.

However the quantum yield of the PL of si nanocrystal is larger by several orders of magnitude than the bulk si due to quantum confinement, so starting from the bulk, it is expected that the PL yield will increase when one goes to nanostructure. The low yield observed in larger sample is consistent with a spatial confinement model where the photoluminescence yield is expected to decrease with size because the probability of finding defect in the crystallite increases considerably, however in nanocrystal the spatial confinement by potential barriers prevents the diffusion of exciton to non-radiative centers. In systems of si-nc, one can additionally take the advantage of high quality oxide to passivate the surface and therefore eliminate many nonradiative channels, such as dangling bonds and defect centers. This further enhance the quantum efficiency by reducing the total decay rate.

2.3 Oscillator strength

Oscillator strength is particularly useful as a method of comparing transition strength between different types of quantum mechanical system, and it used to calculate transition probabilities, dipole matrix elements, and etc.

Consider f_{ij} to be the oscillator strength associated with Z electron transitions from the ground state to an excited states. If this system is irradiated with a spectrally uniform power density over all of its transitions, the total absorption power would be due to transition from initial state to final state. Since oscillator strength defined interims of single oscillator, the sum of the oscillator strength must be summed up to Z. $\Sigma_{i \neq j} f_{ij} = Z$, however if we consider $\mid i >$ to be an excited state, we realize that we can have transitions that result in emission as well as absorbtion. Since oscillator strength was defined in terms of absorption. The value will be negative for transition, that radiate power back in to radiation field. This will result in oscillator strength greater than unity since they were defined interims of net power absorbed. Therefore

$$\Sigma_{i \neq j} f_{ij} \geq Z \; absorption$$

$$\Sigma_{i \neq j} f_{ij} \leq 0 \; emission$$

The quantum confinement effect changes the energy level continuum in the bulk material in to a discrete level structure namely the sub-band structure. This leads to the enhancement of the oscillator strength of the exciton through increased spacial overlap between the electron and the hole. The dielectric confinement also enhances the exciton binding energy and the exciton oscillator strength for dots having size of the order of exciton bohr radius.

2.4 Nonlinear optical responses

Semiconductor materials have been widely studied in recent years for their potential use in non linear optical devices. Bulk crystalline silicon is not known to be the nonlinear material of choice due to the long lifetime of its carriers and indirect band gap in the near infrared spectral region, with very low emission efficiencies, however at the nanoside dimensions silicon exhibits sizeable non linear effects. In typical semiconductor nanocrystals, energy level spacing in the order of about 0.2 eV, depending on the material and quantum number. If the integrated oscillator strength over a range of 0.2 eV compressed in to line width of a few meV, then applicability for non-linear optical devices and applications become a reality. One can consider the refractive index (n) and the absorption coefficient (α) as $n = n_0 + n_2(I)$ and $\alpha = \alpha_0 + \beta(I)$, where n_0 and α_0 are the linear terms discussed before, while $n_2(I)$ and $\beta(I)$ are the nonlinear refractive index and nonlinear absorption coefficient , respectively, and I is intensity of the pump beam. This mechanism is intrinsically very fast. However, in a semiconductor, other kind of nonlinearities are present due to thermal lansing effects and free carrier effects [12]. Measurements on

si-nc have demonstrated that all kinds of nonlinearities are present and one can distinguish them by using different wavelengths of the excitation light pulses. For very short (fs) light pulse, kerr nonlinearity dominates [12]. In this case, the nonlinearities are due to the polarization of the strained bonds at the interface of the si-nc can not be discarded. Nonlinear absorption effect in si-nc are mostly due to two-photon absorbtion. They are particularly determined because, when two photon absorption present, it generates a large amount of excited carriers which intern absorb light by excited carrier absorption but also cause, via a Kramers-Kroning transformation, excited carrier refraction which affects $n_2(I)$.

In the next chapter we present quantitative description of optical parameters by varying the size of nanocrystal and laser pump flux.

Chapter 3

Analytical calculation for optical parameters

Changing the size of nanocrystal and varying the pump flux strongly affect the probability for radiative de-excitaton rate, PL intensity, quantum efficiency and radiative lifetime among the others, thus in this chapter we will derive a theoretical formulations of size dependent radiative recombination rate, PL intensity, quantum efficiency and radiative lifetime in the low and high pump laser flux regimes by simple mathematical expressions.

3.1 Non-radiative recombination rate

In parallel with radiative transition, non radiative process occur in nc-si. Nonradiative process play a problematic role in nc-si, due to their high recombination rates which substantially exceed the rates of radiative transitions [1]. Among the possible non-radiative process, capture on dangling bonds and Auger recombination are the most efficient. Both process are phonon-assisted, and quench the luminescence in nc-si [1].

Dangling bonds can produce deep lying states in the nc-si band structure, these states trap the excited electron and hole prior to their recombination, therefore the emission energy of nc-si is predicted to depend strongly on the number and nature of bonds on the nc surface.

When carriers escape from the confined zone to more extended or less passivated regions, non-radiative recombination can occur. Both carriers, electrons and holes can tunnel, but generally holes are more localized because the potential barriers are higher. The exponential dependence of non-radiative decay rate with confined energy is approximated by tunnelling of electrons through barrier whose thickness and height are "a" and "v" respectively, so that $\Gamma_{nr} = \alpha \exp(\frac{E}{\beta})$ with $\alpha = \exp(-\frac{2a\sqrt{m(v+Eg/3)}}{\hbar})$ and $\beta = (\frac{3\hbar}{a})\sqrt{\frac{(v+Eg/3)}{m}}$ where m is the effective mass of the electron inside the barrier material and E_g is the bulk energy gap [13]. Thus the low- energy (infrared) part of photoluminescence spectrum has an exponential tail.

3.2 Stretched exponential decay model

In studying the photoluminescence decay behavior different authors found very different time constants and different decay rates of exponential, double-exponential, stretched exponential and non-exponential types [14]. Fitting the decay curve with double-exponential, triple-exponential and higher exponential models would imply an erroneous assumption of two or more discrete lifetimes [14], So that its use can not be justified from physical point of view. The stretched exponential provides continuous lifetime distribution due to a range of micro environments and fit better to the decay curves. The stretched exponential function is known us kohlrausch-Williams watts function, the stretched exponential function was first studied by kohl rausch in 1847 as an empirical description for the structural relaxation of glassy fibers and sequently used by G.Williams and D.C Watts to describe dielectric relaxation in polymers. Since then, a large number of relaxation systems ranging from earth quakes, galactic light emissions, and biological extinction to economic and scientific citations have been found to exhibit this type of function [14]. $f(t) = (\frac{\beta}{t}) \exp(-(\Gamma t)^{\beta})$ where Γ -is the experimental decay rate which is equal to the sum of radiative and non- radiative de-excitation rates, β varies between 0 and 1, the

value illustrates how close the decay curve is to single exponential. when the value of $\beta = 1$ the decay curve is single exponential which implies that, at a given frequency, all the nanocrystals emit light with the same rate. The decay curves are obtained by time-correlated single photon counting and the average time between the start pulse and the stop pulse (i.e photon arrival time) is calculated from the experimental data. For single exponential decay this is equal to the decay time.

3.3 Average lifetime

In this section we are going to calculate the average lifetime of the total de-excitation rate.

At time t we have N(t) recombination from N(0) bound electron-hole pairs (exciton) and at time t + dt we still have N(t)+ dN(t) recombination, hence dN(t) recombination at time between t and t+ dt, and $dN(t) < 0$ which means that the number of exciton progressively depleted due to electron-hole recombination. From the above statements we have the following relations.

-$dN(t) \sim dt$ and $dN(t) \sim N(t)$, now bringing the two proportionalities in to one equation gives -$dN(t) \sim N(t)dt$. To change proportionality in to equality, we introduce a constant Υ, the above equation can be written as $\frac{dN(t)}{dt} = -\Upsilon N(t)$

But integration of the above equation gives exponential function which represents spontaneous decay. However, the presence of electrostatic force that capture excitations, which changes the rate of spontaneous decay to time dependent decay rate which can stretch the decay

$$\frac{dN(t)}{dt} = -\Upsilon \frac{N(t)}{t^{\alpha}}$$

Rearranging and integration of the above equation gives $N(t) = N(0)\exp(-(\Gamma_{exp}t)^{\beta})$, where N(t) is electron hole recombination at time t and N(0) is the total number of

exciton at time t =0. Γ_{exp} is experimental decay rate which is the sum of radiative and non-radiative de-excitation rate and β is parameter between 0 and 1.

The average lifetime of the total de-excitation is defined as

$$\tau_{av} = \frac{total\ time\ taken\ for\ de-excitation}{total\ number\ of\ excitons\ at\ t=0}$$

Mathematically,

$$\tau_{av} = -\frac{1}{N(0)} \int_0^\infty t\ dN(t)$$

and,

$$dN(t) = d(N(0)\exp(-(\Gamma_{exp}t)^\beta))$$

After integration, we get $\tau_{av} = \frac{\Gamma'(1+\frac{1}{\beta})}{\Gamma_{exp}}$ where Γ' is gamma function, therefore the average lifetime of the de-excitation is given by

$$\tau_{av} = \frac{\Gamma'(1+\frac{1}{\beta})}{\Gamma_{exp}}$$

3.4 Effect of Size and laser pump flux on optical parameters

The rate of spontaneous emission determines the statistics of the out put of a single photon source [15], next we will derive the probability for radiative recombination rate by using time dependent perturbation theory.

Assuming that the intensity of the electromagnetic radiation is sufficiently small that the interaction of an electron and radiation can be treated by perturbation theory. The Hamiltonian of an electron that interact with electromagnetic field is $H = \frac{(p+eA)^2}{2m} + V(r)$.

Since the intensity of the field is low, we can ignore A^2 term. Therefore the interaction Hamiltonian can be written as

$$H_{int} = \frac{e(A.P)}{mc}$$

Using time dependent perturbation theory the transition probability of an electron from valence state $|v>$ to conduction state $|c>$ given by Firmi's golden rule as

$$\Gamma = \frac{2\pi}{\hbar}| < c|H_{int}|v > |^2 \delta(E_c - E_v - \hbar\omega)$$

A transition rate depends up on the strength of the coupling between the initial and final states of a system and up on the number of ways the transition can happen (i.e the density of final states). A transition proceed more rapidly if the coupling between the initial and final states is stronger. This coupling term traditionally called "matrix element for transition". The interband matrix element of H_{int} for absorption process can be expressed as

$< c|H_{int}|v >= \frac{eA_0}{m} < c|p|v >$, where p is the momentum matrix along A .

$$< c|p|v >= \int \exp(-ik'.r) U'_{k'}(r)\ p\ \exp(ik.r) U_k(r) d^3r$$

$$= \sum \int \exp(i(k-k').r)\ U'_k(r)\ (ik+p)\ U_k(r) d^3r$$

$$= \sum \int exp(i(k-k').r)\ U'_{k'}(r)\ ik\ U_k(r) d^3r + \sum \int \exp(i(k-k').r)\ U'_{k'}(r)\ p\ U_k(r) d^3r$$

The summation arose from dividing the crystal into unit cells, and the first term vanish due to orthogonality of $U'_{k'}(r)$ and $U_k(r)$. Using the periodicity of $U_k(r)$, $r = R + x$. $U(r) = U(x)$

$$< c|p|v >= \frac{1}{\sqrt{\Omega}} \int U'_{k'}(r)\ p\ U_k(r)\ d^3r$$

Introducing, $P = \frac{1}{\sqrt{\Omega}} \int U'_{k'}(r)\ p\ U_k(r)\ d^3r$

$\Gamma = \frac{2\pi e^2}{\hbar m^2} A_0^2 P^2 \delta(E_v - E_c - \hbar\omega)$. The total probability of transition from the valence band to conduction band is obtained by summing Γ over k' and k.

$$\Gamma = \frac{e^2\Omega}{8\pi^2 m^2 \hbar} A_0^2 P^2 \int \delta(E_v - E_c - \hbar\omega)\ f_c(1 - \ f_v) d^3k$$

f_c and $1 - f_v$ are Fermi-dirac distributions. Introducing a dimensionless quantity oscillator strength which is the measure of strength of quantum mechanical transition between two atomic levels.

$$f_{v\to c} = \frac{2}{\hbar m\omega} | < c|p|v > |^2$$

In terms of oscillator strength, Γ can be expressed as

$$\Gamma = \frac{e^2 A_0^2 \omega}{16\pi^2 m} \sum f_{v\to c} \int \delta(E_v - E_c - \hbar\omega) d^3k$$

Several excitation process are possible between different sub-bands for a given optical excitation energy. When electrons are excited with kinetic energies much higher than the temperature of the lattice, they are called hot electrons. These electrons form non-degenerate electron gas and distribute above the bottom of the conduction band after energy relaxation, therefore the photons are emitted with energy higher than the energy of emission which start exceeding the band gap.

Transition between the different valence bands in to different E(k) values of the conduction band are possible near k=0. The transition between top of one valence band to the bottom of the lowest conduction band when both lie at k=0 is responsible for the direct absorption edge, hence for radiative de-excitation. Taking parabolic approximation of both bands we have $E_c - E_v = E_g(r) + \frac{\hbar^2 k^2}{2\mu}$, where $\mu^{-1} = m_e^{-1} + m_h^{-1}$. m_e and m_h are electron and hole mass respectively.

Therefore, the radiative transition rate is $\Gamma_{rad} = \frac{e^2 A_0^2 \omega}{16\pi^2 m} (\frac{2\mu}{\hbar^2})^{\frac{3}{2}} (\hbar\omega - E_g(r))^{\frac{1}{2}} \sum f_{v\to c}$

Let $\chi = \frac{e^2 A_0^2 \omega}{16\pi^2 m} (\frac{2\mu}{\hbar^2})^{\frac{3}{2}}$. Therefore,

$$\Gamma_{rad} = \chi(\hbar\omega - E_g(r))^{\frac{1}{2}} \sum f_{v\to c} \tag{3.4.1}$$

It is found experimentally that the oscillator strength in the nanocrystal is dependent on the crystallite size as the inverse power law, $f_{v\to c} \sim \frac{1}{d^{\beta}}$, where d is the diameter of the spherical crystallites and the power exponent β depends on the material property as well as range of the crystallite size being used, and the value of β is $5 \leq \beta \leq 6$ [7].

If there are N* excited centers in the nanostructure, and if we think of each excited centers contribute at least one photo excited carrier to the nanocrystal then the total oscillator strength is equal to the product of N* and oscillator strength for a single transition of electron from conduction to valence band.

$$\Sigma f_{v\to c} \sim \frac{N^*}{d^{\beta}} \tag{3.4.2}$$

Then the radiative de-excitation rate take the form

$$\Gamma_{rad} \sim \frac{\chi(\hbar\omega - E_g(r))^{\frac{1}{2}} N^*}{d^{\beta}} \tag{3.4.3}$$

Increasing the laser pump flux from smaller to a certain saturation value (to the extent of increasing laser pump flux has no significant effect in increasing the radiative de-excitation rate and PL intensity) enhances the probability for radiative de-excitation rate and PL intensity in nc-si.

For a given photon flux Φ, the photoluminescence intensity of N optically active emitting centers (number of atoms) in nanocrystal is directly proportional to the product of the number of excited centers, N*, and the radiative decay rate, Γ_{rad}. In particular ,under steady-state conditions , an analysis of the two-level system yields

$$I_{PL} \sim N^*\Gamma_{rad} = N\Gamma_{rad}(\frac{\sigma\Phi}{\Gamma_{exp} + \sigma\Phi}) \tag{3.4.4}$$

where σ is the excitation cross section of emitters, and the experimental decay rate, $\Gamma_{exp} = \Gamma_{rad} + \Gamma_{nr}$, comprises the radiative as well as the nonradiative de-excitation paths [2, 4, 16].

3.4.1 For low laser pump flux regime ($\sigma\Phi << \Gamma_{exp}$)

In this section we are going to see the effect of low pump flux on the probability for radiative de-excitation rate, and we also see the influence of probability for radiative de-excitation rate on radiative lifetime, PL intensity, and quantum efficiency of nc-si.

As describe in section 2.1, the surface polarizartion effect theory considers the nanostructure to have two regions, surface and core with different dielectric values.

The difference in dielectric constant between the surface and core region of nc-si causes difference in refractive index, thus parts of the low energy incident electromagnetic wave that are not absorbed by surface atoms reflect back instead of going in to the core and there is a probability for surface atoms to absorb the reflected electromagnetic wave, so that the majority of incident electromagnetic waves are absorbed by atoms near and at the surface of the spherical nanocrystal, thus those atoms at the surface and near the surface are active contributors of photoexcited carriers to the nanocrystal.

Probability for radiative de-excitation rate

As the surface area of the spherical nanocrystal increases, the number of atoms at the surface and near the surface increases, and if we think of each atoms contribute at least one photoexcited carrier to the nanocrystal, the number of photoexcited carriers (N^*) are proportional to the surface area ($\sim d^2$) of nc-si, where d is the diameter of the spherical nanostructure. Since Φ is constant for a given photon flux, then equation 3.4.3 take the form $\Gamma_{rad} = \alpha \frac{e^2 A_0^2}{16\pi^2 m} (\frac{2\mu}{\hbar^2})^{\frac{3}{2}} (\hbar\omega - E_g(r))^{\frac{1}{2}} \frac{1}{d^{\beta-2}}$, where α is the proportionality constant.

Or,

$$\Gamma_{rad} \sim \frac{(\hbar\omega - E_g(r))^{\frac{1}{2}}}{d^{\gamma}} \; where \; 3 \leq \gamma \leq 4.$$

Radiative lifetime

The radiative lifetime which is the lifetime of an excited electron in the presence of light emission transition is the reciprocal of probability for radiative de-excitation rate. Therefore

$$\tau_{rad} \sim \frac{d^{\theta}}{(\hbar\omega - E_g(r))^{\frac{1}{2}}} \; where \; 3 \leq \theta \leq 4. \tag{3.4.5}$$

photoluminescence intensity

Under this condition PL intensity is proportional to the internal quantum efficiency ($I_{Pl} \sim N\eta\sigma\Phi$). Since the number of excited centers (N*) are proportional to the surface area of the nanostructure ($\sim d^2$), and $\sigma\Phi$ is constant for constant photon flux, then equation 3.4.4 take the form $I_{pl} = \xi\ \sigma\Phi\frac{(\hbar\omega - E_g(r))^{\frac{1}{2}}}{d^{\beta-2}}$, where ξ is proportionality constant.

Or

$$I_{PL} \sim \frac{(\hbar\omega - E_g(r))^{\frac{1}{2}}}{d^{\nu}} \; where \; 3 \leq \nu \leq 4 \tag{3.4.6}$$

3.4.2 For high laser pump flux regime ($\sigma\Phi >> \Gamma_{exp}$)

In this section we are going to see the effect of high pump flux on the probability for radiative de-excitation rate, and we also see the influence of probability for radiative de-excitation rate on radiative lifetime, PL intensity, and quantum efficiency of nc-si.

Probability for radiative de-excitation rate

In this regime the intensity of the pump flux is high, thus it able to excite those atoms at the core of the spherical nanocrystal, and we can regard the number of atoms in the nanocrystal as active contributors of photoexcited carriers. Now the excitation is due to contribution of volume of the nanostructure ($\sim d^3$), then the radiative de-excitation

rate take the form $\Gamma_{rad} = \varphi \frac{e^2 A_0^2}{16\pi^2 m} (\frac{2\mu}{\hbar^2})^{\frac{3}{2}} (\hbar\omega - E_g(r))^{\frac{1}{2}} \frac{1}{d^{\beta-3}}$, where φ is the proportionality constant.

Or

$$\Gamma_{rad} \sim \frac{(\hbar\omega - E_g(r))^{\frac{1}{2}}}{d^{\gamma}} \; where \; 2 \leq \gamma \leq 3$$

Radiative lifetime

Then, the enhanced radiative lifetime in high pump laser flux regime can be expressed as

$$\tau_{rad} \sim \frac{d^{\gamma}}{(\hbar\omega - E_g(r))^{\frac{1}{2}}} \; where \; 2 \leq \gamma \leq 3 \tag{3.4.7}$$

Photoluminescence intensity

In this regime PL intensity is proportional to the product of the number of optically active emitting centers (N) and the radiative recombination rate. $I_{PL} \sim N\Gamma_{rad}$, then the size dependence of PL intensity take the form

$$I_{PL} \sim \frac{(\hbar\omega - E_g(r))^{\frac{1}{2}}}{d^{\rho}} \; where \; 2 \leq \rho \leq 3 \tag{3.4.8}$$

However, when the excitation pump is very high and several electrons in the dot are excite, then the Auger recombination become possible. Since Auger interactions are fast, the radiative channel will be "shunted" in this case, and also the nanocrystal-nanocrystal interaction which causes the excited electrons tunnel out from the confined zone to another become prominent.

3.5 Quantum efficiency

An internal quantum efficiency $\eta = \frac{\Gamma_{rad}}{\Gamma_{exp}}$ is the "weight" of the radiative channel in the recombination process [1] or the measure of the fraction of probability of the total de-excitation which radiatively recombine. Where Γ_{exp} is the experimental decay

rate which comprises the radiative (Γ_{rad}) and non-radiative (Γ_{nr}) de-excitation paths ($\Gamma_{exp} = \Gamma_{rad} + \Gamma_{nr}$) which can be frequency dependent. The increase in probability for radiative de-excitation rate increases the quantum yield, however when the probability for non-radiative de-excitation is dominant mechanism in the recombination process, the quantum efficiency gets smaller. An internal quantum efficiency of a nanocrystal is only limited by its internal property, while the external quantum efficiency is $N^*\eta$ where, N^* is the proportion of emitted crystallites.

Next, we will derive the size dependence of internal quantum efficiency.

From equation 3.4.3 we have

$$N^*\Gamma_{rad} \sim \chi(\hbar\omega - E_g(r))^{\frac{1}{2}}(\frac{N^*}{d^\beta}) \tag{3.5.1}$$

From equation 3.4.4 we have

$$N^*\Gamma_{rad} = N\Gamma_{rad}(\frac{\sigma\Phi}{\Gamma_{exp} + \sigma\Phi}) \tag{3.5.2}$$

plugging this in to equation 3.5.1 we have

$$N\Gamma_{rad}(\frac{\sigma\Phi}{\Gamma_{exp} + \sigma\Phi}) \sim \chi(\frac{N^*(\hbar\omega - E_g(r))^{\frac{1}{2}}}{d^\beta}) \tag{3.5.3}$$

For low laser pump flux regime ($\sigma\Phi << \Gamma_{exp}$) equation 3.5.3 reduced to $N\sigma\Phi\eta \sim \chi(\hbar\omega - E_g(r))^{\frac{1}{2}}N^*(\frac{1}{d^\beta})$, where η is the internal quantum efficiency ($\eta = \frac{\Gamma_{rad}}{\Gamma_{exp}}$)

Then

$$\eta \sim \chi(\frac{N^*}{N})\frac{(\hbar\omega - E_g(r))^{\frac{1}{2}}}{\sigma\Phi d^\beta} \tag{3.5.4}$$

For low laser pump flux regime those atoms at the surface are active participator in the contribution of photoexcited carriers to the nanostructure. Hence the number of excited centers (N*) are proportional to the surface area of the nanostructure ($\sim d^2$) and the number of optically active emitting centers are proportional to the volume of

nanocrystal ($\sim d^3$), where d is the diameter of the spherical nanostructure. Then equation 3.5.4 take the form of $\eta \sim \frac{\chi(\hbar\omega - E_g(r))^{\frac{1}{2}}}{\sigma\Phi} d^{-(\beta+1)}$ where $\chi = \frac{e^2 A_0^2 \omega}{16\pi^2 m}(\frac{2\mu}{\hbar^2})^{\frac{3}{2}}$. Since χ and $\sigma\Phi$ are constant for a given external pump flux and then, the internal quantum efficiency $\eta \sim \frac{(\hbar\omega - E_g(r))^{\frac{1}{2}}}{d^{\beta+1}}$ for low pump regime.

Or

$$\eta \sim \frac{(\hbar\omega - E_g(r))^{\frac{1}{2}}}{d^{\lambda}} \; where \; 6 \leq \lambda \leq 7 \tag{3.5.5}$$

For low laser pump flux regime, the internal quantum efficiency has inverse power relation with the diameter of the nanostructure (equation 3.5.5), the value of λ determined by material property, range of the nanocrystal being used and the strength of the external pump flux. Therefore the internal quantum efficiency increases when the diameter of the nanostructure decreases and vice-versa.

3.6 Frequency dependent peak value of optical parameters

Maximizing the size dependent optical parameters that we obtain in equations 3.4.6, 3.4.8, and 3.5.5 we can get the diameter associated with the peak value of optical parameters (d_{max}) as

$$d_{max} = 2.578(\frac{1 + \frac{1.39}{2\alpha}}{\hbar\omega - E_g(bulk)})^{\frac{1}{1.39}} \tag{3.6.1}$$

As described in equations 3.4.5 and 3.5.5, in low pump flux regime, α has values $3 \leq \alpha \leq 4$, and $6 \leq \alpha \leq 7$ for PL intensity and internal quantum efficiency respectively, and $2 \leq \alpha \leq 3$ for PL intensity in high pump flux regime (equation 3.4.8).

The maximum energy associated with each optical parameters as a function of excitation frequency is

$$E_{max} = E_g(bulk) + \frac{\hbar\omega - E_g(bulk)}{1 + \frac{1.39}{2\alpha}} \tag{3.6.2}$$

Equation 3.6.1 shows that, we can not simultaneously achieve maxima of PL intensity and internal quantum efficiency due to difference in value of α. Expanding equation 3.6.2 as a power series and taking the first order approximation gives

$$E_{max} \approx \hbar\omega - \frac{0.695}{\alpha}(\hbar\omega - E_g(bulk)) \tag{3.6.3}$$

From equation 3.6.3 we can see that PL energy is always less than the excitation energy, and when the oscillator strength is large (value of α is large) PL energy gets larger.

Using fortran programming we generate graphs of equations 3.4.5, 3.4.6, 3.4.7, 3.4.8 and 3.5.5 as a functions of PL wavelength, PL energy and size, and thus the codes to generate the graphs are available in the appendix.

Chapter 4

Results and discussions

In this chapter we are going to discusses on the pump flux and size dependence of optical parameters that we obtain in equations 3.4.5, 3.4.6, 3.4.7, 3.4.8 and 3.5.5.

Oscillator strength, PL intensity, probability for radiative de-excitation rate, radiative lifetime and quantum efficiency are among the parameters that describe the luminescence property of a given crystallite. These parameters have strong size dependent property, hence tuning the size of nanocrystals strongly affect their magnitude. When the size of nc-si is comparable to its characteristics bohr exciton radius (4.9 nm), the phonon assisted indirect band gap transition is turn into direct band gap transition and the probability of finding defect and impurity states in the band also minimize, and thus the probability for radiative de-excitation rate and quantum efficiency of the nanocryatal increases, in effect PL intensity that we get from the nanocrystallite increases appreciably.

4.1 Internal quantum efficiency

From our results that we obtain in equation 3.5.5, we find that for spherical nanocrystal with diameter d, the internal quantum efficiency has inverse power relation with the diameter. The power exponent (λ) can be determined by material property, range of the nanocrystal being used and the strength of the external pump flux. This result confirms that the increase in overlap of electron and hole wave functions as a consequence of size reduction increases the radiative recombination rate in nc-si. The improvement in

radiative de-excitation channel enhances the internal quantum efficiency drastically.

4.1.1 Graphs of internal quantum efficiency

From the graph of normalized internal quantum efficiency versus size of the nanocrystal we can see that when the excitation laser pump flux is very high and the size of nanocrystal is smaller and smaller, the population of nanocrystal with internal quantum efficiency near and at the peak values falls rapidly and very small portion of the nanocrystal will have significant internal quantum efficiency, the rest have nearly zero internal quantum efficiency. This phenomenon decrease PL intensity obtained from nanocrystal and can be explained in terms of Auger recombination which switch on at higher pump flux regime. The other exciting phenomena that we can see from the graph is that, as the size of the nanodot gets smaller and smaller the slope of internal quantum efficiency versus size graph gets steeper and steeper, which indicates that changing the size a little, strongly alters the internal quantum efficiency of the smallest nanocrystal than larger one.

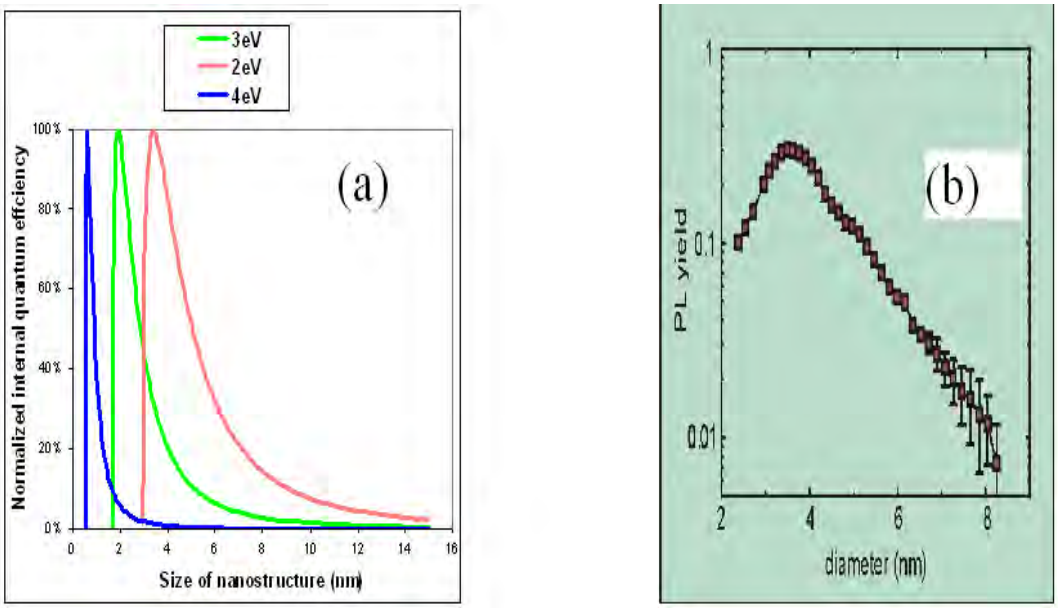

Figure 4.1: Using equation 3.5.5 we simulate the enhancement of internal quantum efficiency as the size decreases. The size dependence of internal quantum efficiency based on our simulation (a) is in well agrement with experimental result (b) which is adapted from [19].

On the other hand, the normalized internal quantum efficiency versus PL energy and wavelength graphs show that PL energy and wavelength that we obtain from smaller dots blue shifted with respect to PL spectra from larger dots due to the effect of quantum confinement. When the size of the dot decreases the band gap stretches and photoexcited carriers in the dot at least gain energy in the order of the band gap, therefore PL energy one can get from smaller dots larger, and thus we can tune the emission spectral range across the visible by using proper sized nc-si.

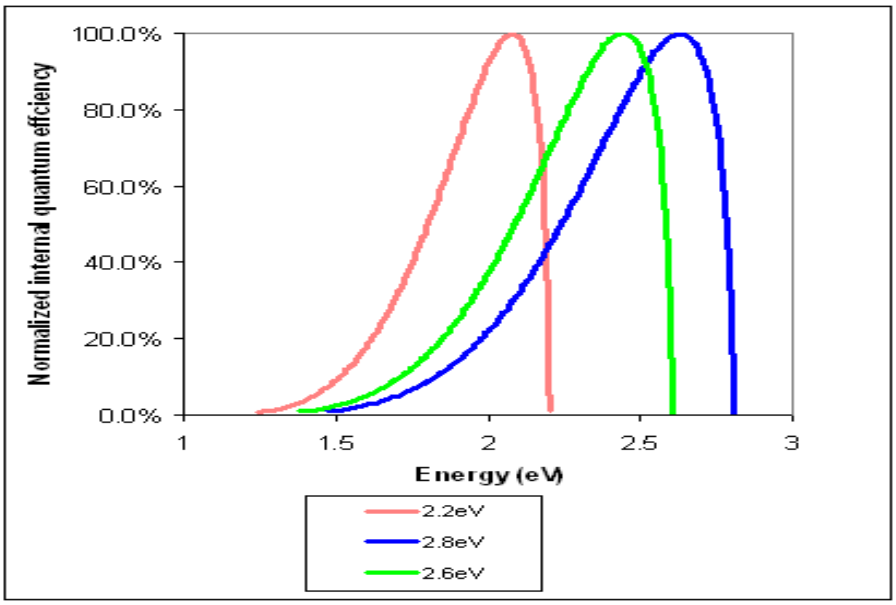

Figure 4.2: The internal quantum efficiency (η) versus energy graphs for smaller dots blue shifted in energy with respect to larger dots.

4.2 Photoluminescence intensity

From our results that we obtain in equations 3.4.6 and 3.4.8, we find that for spherical nanocrystal with diameter d, PL intensity has inverse power relation with the diameter. The power exponents (ν and ρ) can be determined by material property, range of the nanocrystal being used and the strength of the external pump flux. From these results we can enhance PL intensity by miniaturizing the size of nc-si and increasing the excitation laser pump flux.

4.2.1 Graphs of photoluminescence intensity

From the PL intensity versus wavelength and energy graphs, due to reduction in size, the band gap of silicon nanostructures increases involving a blue shift in PL spectra. Quantum confinement effect in the nanocrystal opens up the band gap as well as relaxes the selection rules for radiative transitions, thus it give rise to PL in the visible region for crystallite size below 5nm.

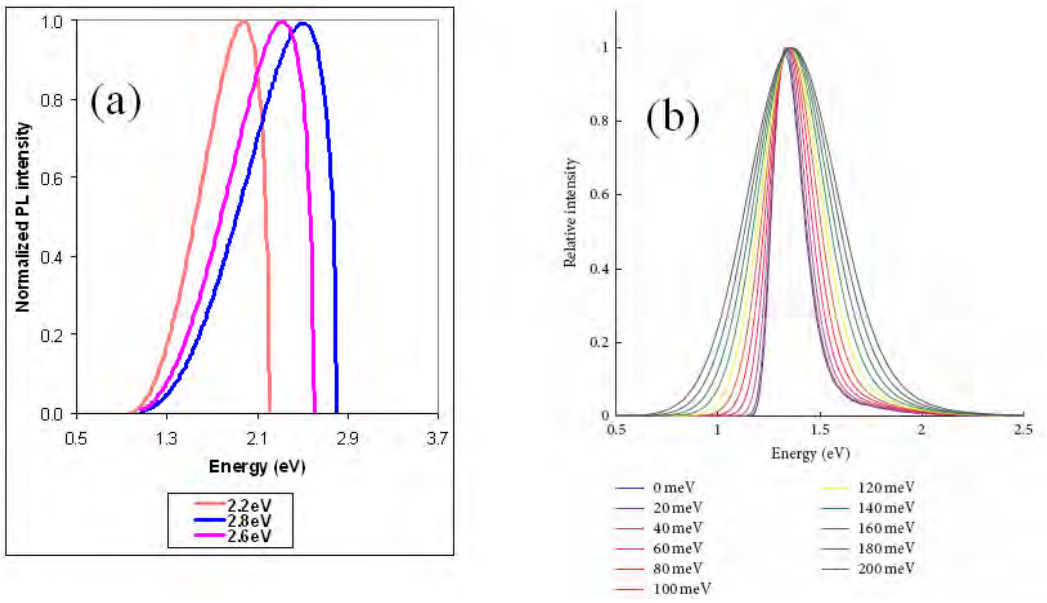

Figure 4.3: From our simulation, the intensity versus PL energy graph for smaller dots blue shifted with respect to larger dots (a) which is in well agrement with experimental result (b) is adapted from [1]

The other advantage of increasing pump flux can be seen in the PL intensity versus energy graph, which causes blue shift in emission spectra. This can be explained as, those nanocrystals with band gap greater than the excitation energy in the ensemble of nc-si inactive in low pump flux regime and when the excitation laser pump flux increases they switch on and give greater energy.

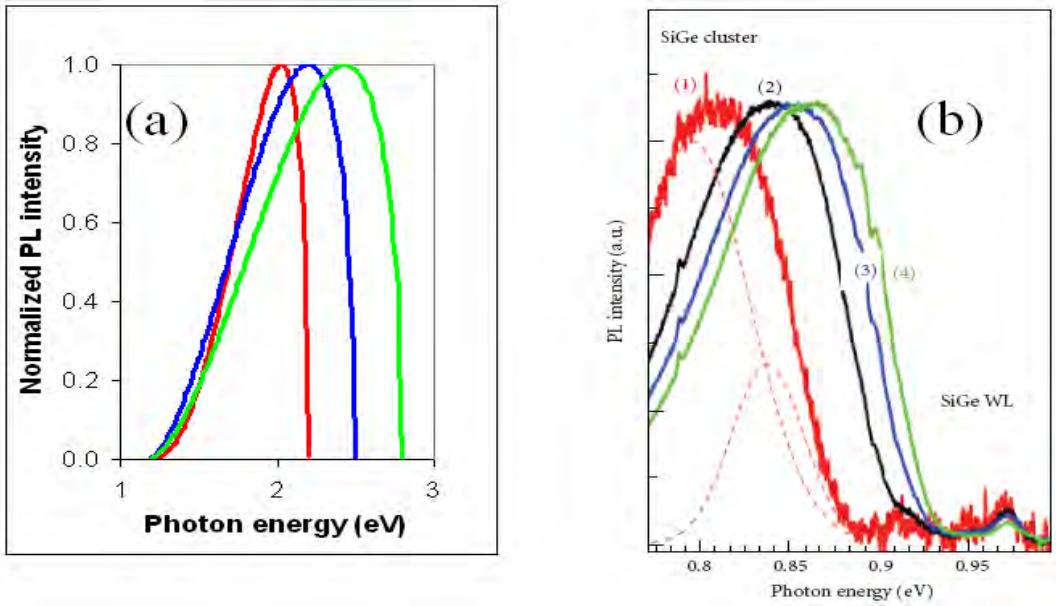

Figure 4.4: Using equations 3.4.6 and 3.4.8 we simulate normalized PL intensity versus PL energy. Under increasing excitation intensity PL shift to higher photon energy, our simulation (a) is in well agrement with experimental results (b) which is adapted from [18] .

4.3 Radiative lifetime

Our result show that the size dependence of radiative lifetime that we obtained in equations 3.4.5 and 3.4.7 have inverse power relation with the diameter of spherical nanocrystal. The power exponents (θ and γ) can be determined by material property, range of the nanocrystal being used and the strength of the external pump flux. These results confirms that miniaturizing the size of nanocrystals increases the overlapping of electron and hole wave functions in position space. This overlapping increases the oscillator strength for transition and this intern improve the radiative lifetime. Additionally increasing the laser pump flux alters the radiative lifetime drastically.

4.3.1 Graph of radiative lifetime

From the graph of radiative lifetime versus size of nanostructure, one can basically understand that the radiative lifetime which is the lifetime of an excited electron in the presence of light emission transition gets smaller and smaller as one goes to smaller size of the dot due to quantum confinement effect. In addition, we can see the advantage of increasing pump flux on the radiative lifetime. Increasing pump flux up to saturation value significantly enhance the radiative de-excitation rate, and thus it alters the radiative lifetime strongly.

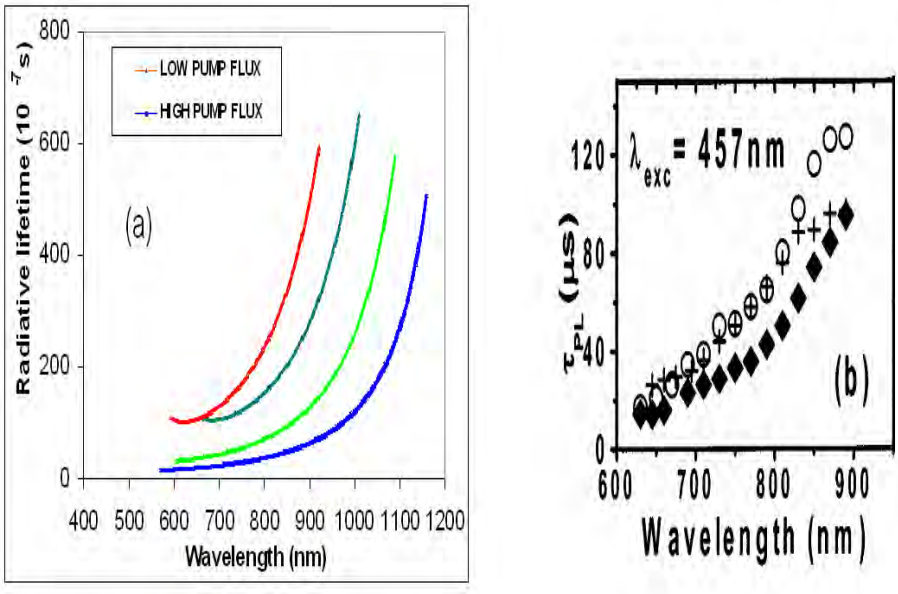

Figure 4.5: Using equations 3.4.5 and 3.4.7 we simulate the decrease in radiative lifetime as the excitation laser pump flux increases and size decreases, thus our simulation of radiative lifetime as a function of PL wavelength (a) is in well agrement with experimental result (b) which is adapted from [17].

4.4 Peak values of optical parameters

It is very important to note that our model is able to predict with what excitation frequency one can optimize quantum efficiency and PL intensity from ensembles of nanocrystal with a given mean diameter. It is clear that the distribution of size in the ensembles of nanocrystal can be approximately Gaussian in shape, therefore the intensity and quantum efficiency strongly influenced by the dominant size distribution in the ensemble. Equation 3.6.1 gives the relation ship between peak values of optical parameters for a given mean diameter in the ensemble of nc-si with excitation frequency, from this equation and from the graphs of optical parameters that we derived earlier one can see that those nanocrystals with energy gap closer to excitation energy show maximum PL intensity and internal quantum efficiency, thus it is worth to use appropriate excitation frequency depending on the energy gap of dominant size distribution.

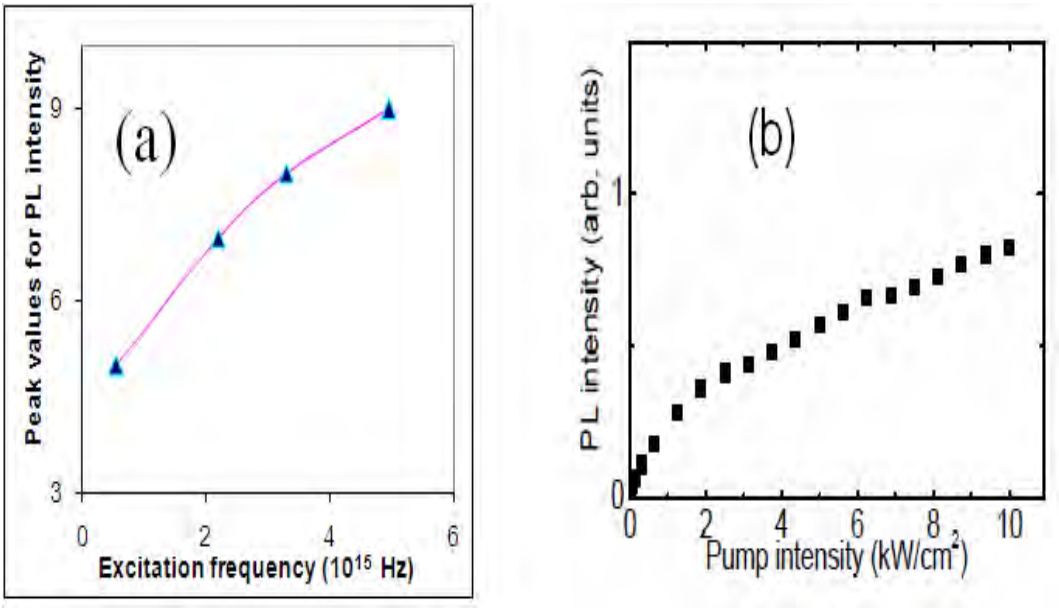

Figure 4.6: Peak value for PL intensity versus frequency of external pump flux our simulation (a) and experimental (b) which is adapted from [19].

Chapter 5

Summary and Conclusion

In this work we have presented the effect of size and pump flux on the PL emission spectra and quantum yield of a silicon nanocrystal. We used quantum confinement and surface polarization effect models to describe the PL behavior of nc-si. The types of the atoms at the surface strongly affect the luminescence behavior of a nanocrystal, however in this work we studied the influence of size and external pump flux on the radiative de-excitation rate, radiative lifetime, PL intensity and internal quantum efficiency of pure silicon nanocrystal.

The low Light emission and quantum efficiency in bulk Si can be enhanced by several order of magnitude when one goes to nanostructure. In silicon nanostructure the phonon assisted indirect band gap transition is turn into direct band gap transition and the probability of finding defect and impurity states in the band also minimize, hence the probability for radiative de-excitation rate and quantum efficiency of the nanocryatal increases. When the size of nanocrystal decreases below its characteristics bohr exciton radius, oscillator strength, PL intensity, probability for radiative de-excitation rate, radiative lifetime and quantum efficiency are strongly depend on the size of nanostructure, hence tuning the size of nanocrystals strongly affect their magnitude, and thus the ability to vary these parameters is a key to realizing nanostructures with novel properties.

Our result shows that, τ_{rad} decreases with decreasing size of nc-si in both low and high pump (to the extent of increasing pump has no significant effect in increasing the

radiative de-excitation rate and PL intensity) flux regimes, however Γ_{rad} , PL intensity, and η increase with decreasing the size of the nc-si in both low and high pump flux regimes, and thus the PL emission intensity and η enhances due to quantum confinement and we can tune the emission spectral range across the visible by using proper sized nc-si. Our model able to predict qualitatively the published experimental data from noncrystalline silicon produced using variety of techniques.

In conclusion, our work presents a new approach for the PL mechanism of nc-si. Our results conform that miniaturizing and increasing laser pump flux enhances the emission intensity and quantum efficiency of nc-si, which in turn play a great role in extraction of high emission power from nc-si. For the future, it is also worth to look at temperature and pressure dependence optical parameters for other silicon nanostructures (quantum wire, quantum well and etc). We can extend our model for detailed temperature dependent calculations. It is important to note that our simple model shows that for smaller dots the radiative lifetime as well as quantum efficiency improved drastically. This is very important for optoelectronic application of nanosilicon. These results are in conformity with some recent investigations.

Appendix

A. This is the FORTRAN 77 code to generate PL intensity and internal quantum efficiency versus PL energy graphs.

Real d,E,QE

Open(1,file='M.dat',status='unknown')

Do D=1.814047,12,0.001

Given=$3 \leq \nu \leq 4$ for PL intensity and $6 \leq \lambda \leq 7$ for internal quantum efficiency

W=Given, hV=2.8

E=$1.17 + 3.73/d**1.39$

QE=$sqrt(hV - E) * d**(-w)$

$Write(1,*)E, QE$

Print*,E,QE

Enddo

End

B. This is the FORTRAN 77 code to generate radiative lifetime versus PL wavelength graph. Real d,E,Gamma rad,Lambda

Open(1,file='L.dat',status='unknown')

Do D=1.914047,12,0.001

W=3.5, hV=2.8

E=1.17+3.73/d**1.39

Gamma rad=sqrt(hV-E)*d**(-w)

Lambda=1240/E, Trad=1/gamma rad

```
Write(1,*)lambda,Trad
Print*,lambda,Trad
Enddo
End
```

C. This is the FORTRAN 77 code to generate size dependence of internal quantum efficiency graph. Real d,E,QE

```
Open(1,file='Y.dat',status='unknown')
do D=1.6691400000,5,0.01
w=6.2, hv=3
E=1.17+3.73/d**1.39
Qe=sqrt(3-E)*d**(-w)
write(1,*)d,QE
print*,d,QE
Enddo
End
```

D. This is the FORTRAN 77 code to generate internal quantum efficiency versus PL wavelength graph. Real d,E,QE

```
Open(1,file='O.dat',status='unknown')
Do D=1.814047,12,0.001
W=6.4, hV=2.8,
Lambda=1240/E
E=1.17+3.73/d**1.39
QE=sqrt(hV-E)*d**(-w)
Write(1,*)Lambda,QE
Print*,Lambda,QE
Enddo
End
```

Bibliography

[1] V. A. Belyakov,V. A. Burdov, R. Lockwood, and A.Meldrum, *Adv. Opt. Tech.*, **ID 279502**, 32(2008).

[2] Robert Joseph Walters and Harry Atwater, Ph.D. thesis, *Silicon Nanocrystals for Silicon Photonics*, California Institute of Technology, 171(2007).

[3] Irrera and Dott. Fabio Iacona, Ph.D. thesis, *Light emitting devices based on silicon nanostructures*, Catania, 187(2003).

[4] Julie Suzanne Biteen and Harry A. Atwater, Ph.D. thesis, *Plasmon-enhanced silicon nanocrystal luminescence for optoelectronic application.*, California Institute of Technology, 184(2006).

[5] W. C. W. Chan, and S. Nie, Science **281**, 2016(1998).

[6] http://W.W.W.ece.nus.edu.sg/coe/, *Nussni Focus Groups 2006 Reasearch Abstract (Nanophotonics)*, (Accessed on 6, March, 2009)

[7] V. Ranjan, Vijay A. Singh, George C. John, *Phys. Rev. B* **58**, 1158(1998).

[8] C. N. R. Rao, A. Muller, A. k. Cheetham, *The Chemistry Of Nanomaterials, **2***, 371-724.

[9] Brian A. Korgel, *SPIE Newsroom*, **10.11172/1200607.0203**, 4(2006)

[10] L. K. Pan, Chang Q. Sun, T. P. Chen, S. Li, C. M. Li and B. K. Tay, *Nanotechnology*, **15**, 180218062004(2004).

[11] Han G. Yoo, Philippe M. Fauchet, *Phys. Rev. B* **77**, 115355(2008).

[12] Min Xie, Zhizhong Yuan, Bo Qian, Lorenzo Pavesi, *Via Sommarive,* ***14***, 2008.

[13] J. C. Via, A. B Siesy, F. Gaspard, R. Herino, M. Ligeon, F. Muller, and R. Romestain, *Phys. Rev. B* **45**, 14174(1992).

[14] K. C. Benny Lee, J. Siegel, S. E. D. Webb, S. Leveque Fort, M. J. Cole, R. Jones, K. Dowling, M. J. Lever, and P. M. W. French, *Biophys J*, **81**, 1265(2008).

[15] A. F. van Driel, G. Allan, C. Delerue, P. Lodahl, W. L. Vos, and D. Vanmaekelbergh, *Phys. Rev. Lett.* **95**, 236804(2005).

[16] Domenico Pacifici, Ph.D. thesis, *Erbium doped silicon nanoclusters for Microphotonics*, Catania, 161(2003).

[17] C. Garcia, B. Garrido, P. Pellegrino, R. Ferre, J. A. Moreno, J. R. Morante, L. Pavesi and M. Cazzanelli, *Appl. Phys. Lett.* **82**, 1595(2008).

[18] L. Tsybeskov, E.-K. Lee, H.-Y. Chang, B. V. Kamenev, D. J. Lockwood, J.-M. Baribeau, and T. I. Kamins, Appl. Phys. Lett. **92**, 033110(2008).

[19] Hans Mertens, Ph.D. thesis, Controlling plasmon-enhanced luminescence, Utrecht University, 160(2007).

[20] Paola Russo, Ph.D. thesis, Production and spectroscopic charicterization of semiconductor cluster films, Catania, 159(2005).